Supporting Information

Layered Birnessite cathode with a displacement/intercalation mechanism for high-performance aqueous zinc-ion batteries

Xian-Zhi Zhai,[†,‡] Jin Qu,*[,†] Shu-Meng Hao,[‡] Ya-Qiong Jing,[†] Wei Chang,[‡] Juan Wang,[†] Wei Li,[†] Yasmine Abdelkrim,[†] Hongfu Yuan,[†] Zhong-Zhen Yu*[,†,‡]

[†] State Key Laboratory of Organic-Inorganic Composites, College of Materials Science and Engineering, Beijing University of Chemical Technology, Beijing 100029, China

[‡] Beijing Key Laboratory of Advanced Functional Polymer Composites, Beijing University of Chemical Technology, Beijing 100029, China

*E-mails: qujin@mail.buct.edu.cn (J. Qu); yuzz@mail.buct.edu.cn (Z.-Z. Yu)

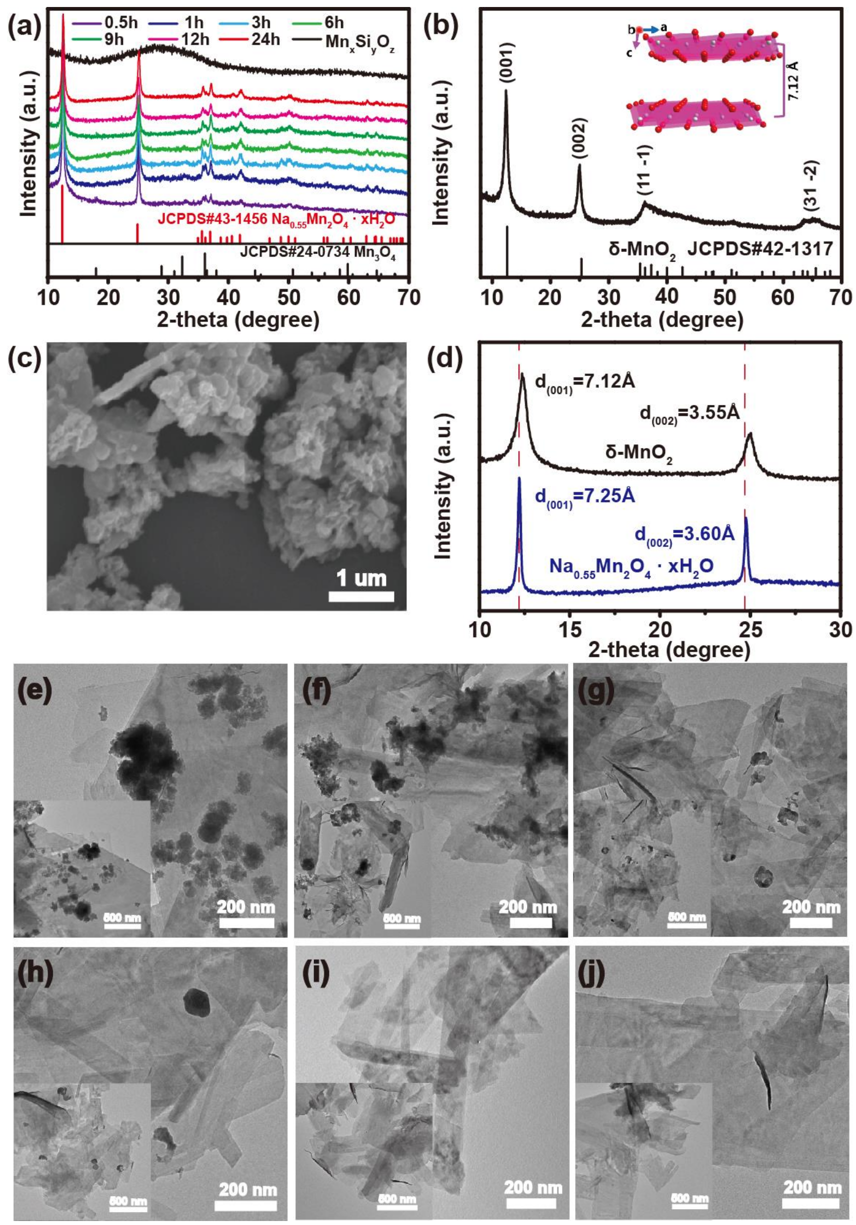

Fig. S1. (a) XRD patterns of the $Mn_xSi_yO_z$ and NMOH with different etching time. (b) XRD pattern of the δ-MnO_2 and an illustration of its crystal structure (inset). (c) SEM image of δ-MnO_2. (d) XRD patterns of NMOH and δ-MnO_2. The TEM images of NMOH with different etching time: (e) 1h, (f) 3h, (g) 6h, (h) 9h, (i) 12h, (j)24h.

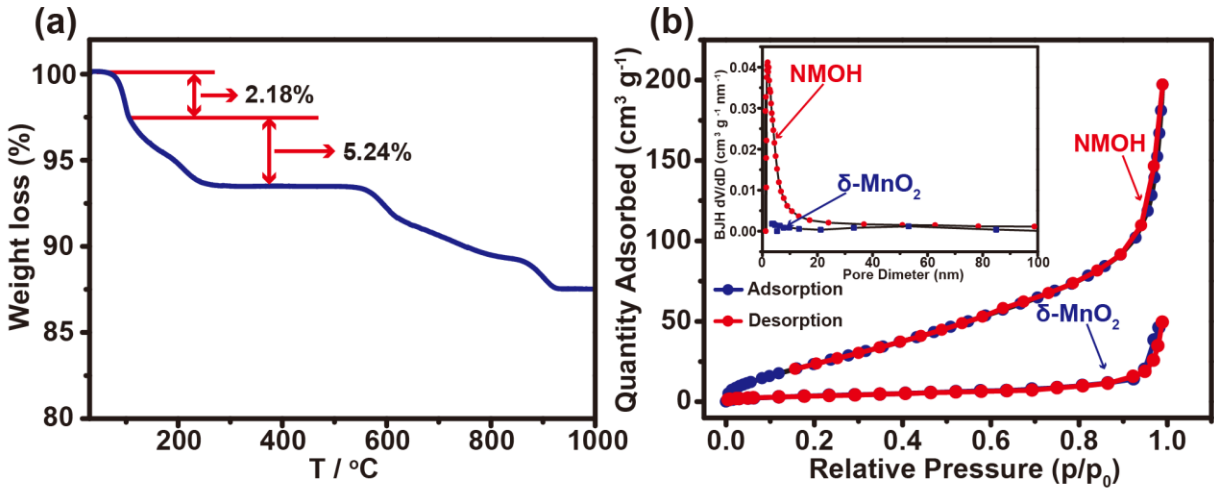

Fig. S2. (a) TGA analysis and (b) Nitrogen adsorption-desorption isotherms of NMOH and δ-MnO_2. The inset is the pore-size distribution calculated using the BJH method (Red: NMOH; Blue: δ-MnO_2). The δ-MnO_2 has a low BET specific surface areas of 13.456 m^2 g^{-1}.

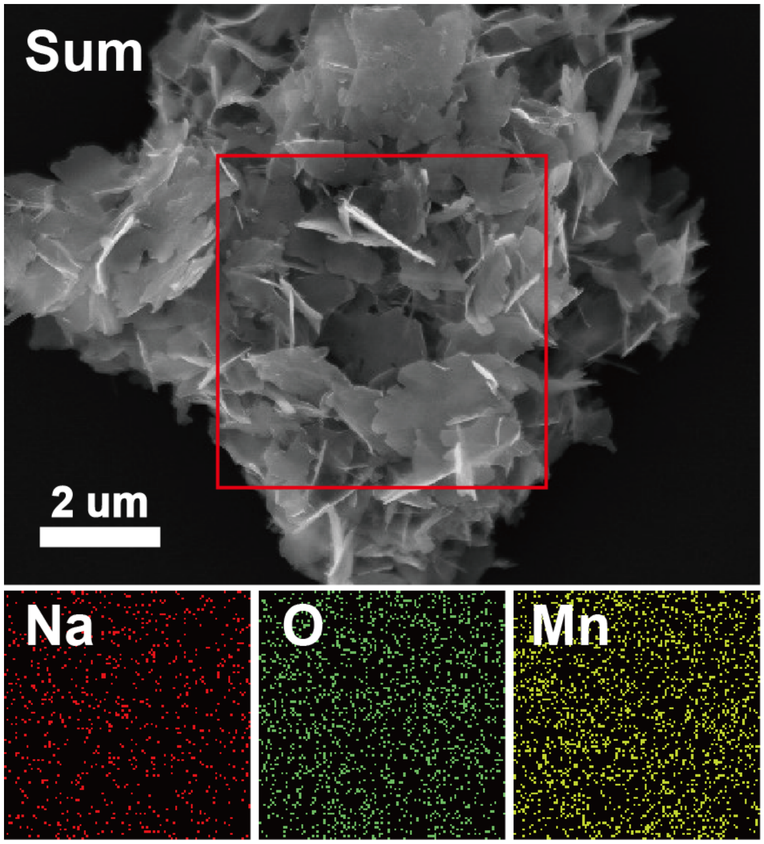

Fig. S3. SEM image and corresponding elemental mapping images of NMOH.

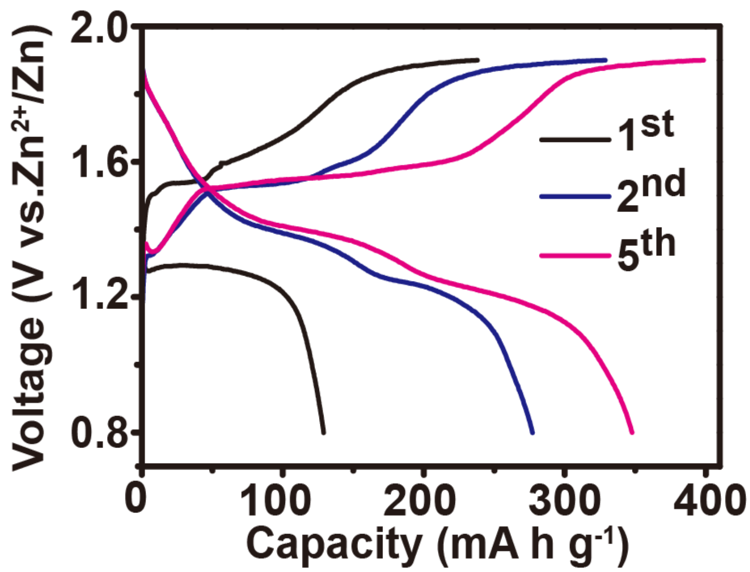

Fig. S4. Galvanostatic charge/discharge profiles of the Zn/NMOH cell tested at a current density of 200 mA g^{-1}.

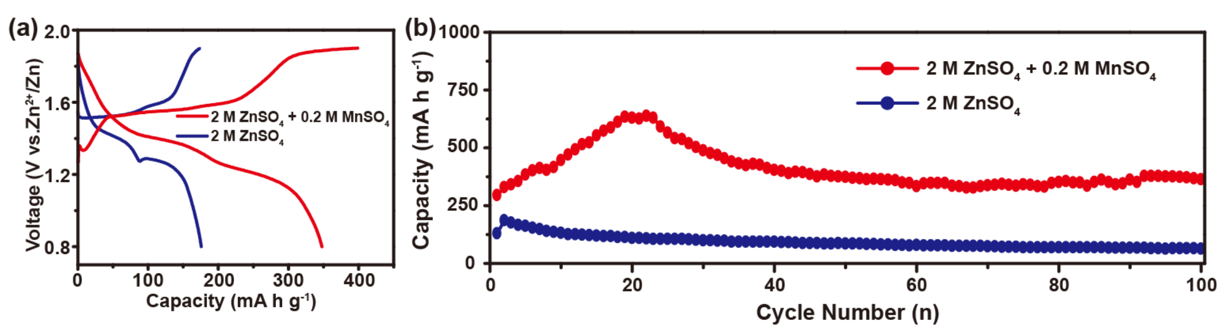

Fig. S5. (a) Galvanostatic charge/discharge profiles and (b) cycling performances of the coin-type Zn/NMOH cell at the current density of 200 mA g^{-1} using an aqueous electrolyte of 2 M $ZnSO_4$ with and without the 0.2 M $MnSO_4$ additive.

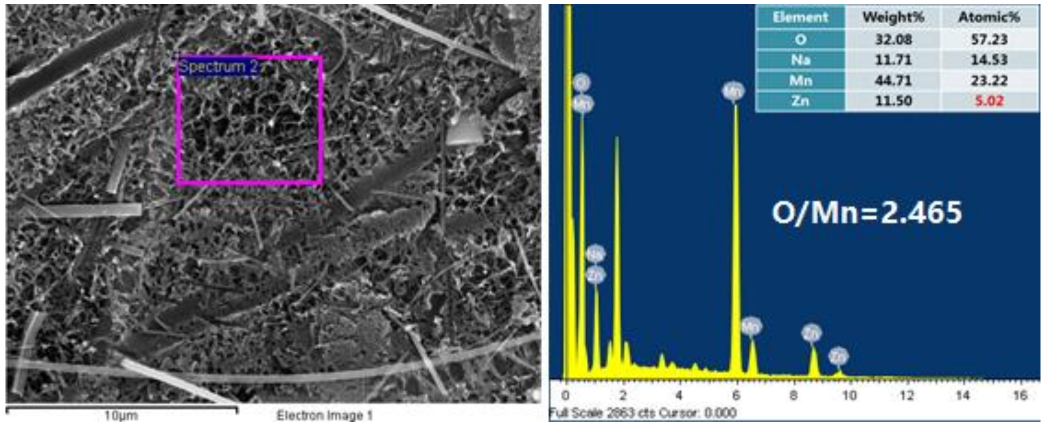

Fig. S6. SEM image and corresponding EDS spectrum of NMOH cathode at fully charged state.

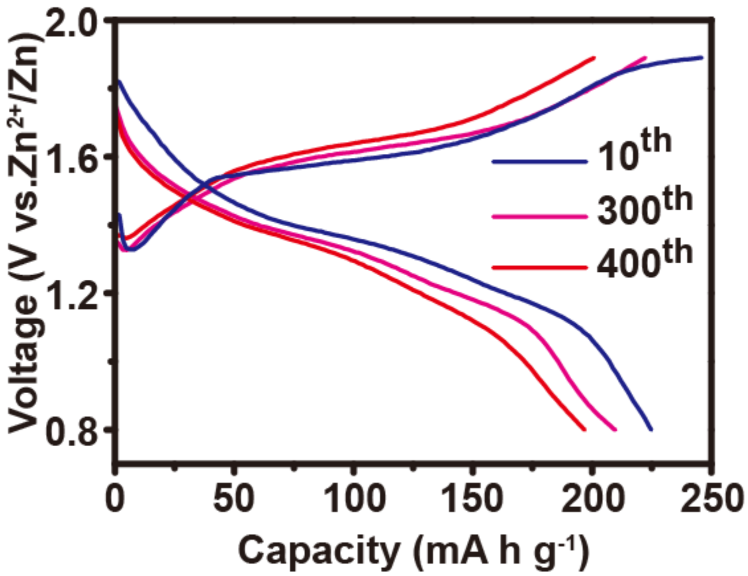

Fig. S7. Galvanostatic charge/discharge curves of NMOH cathode at 500 mA g^{-1} between 0.8 and 1.9 V.

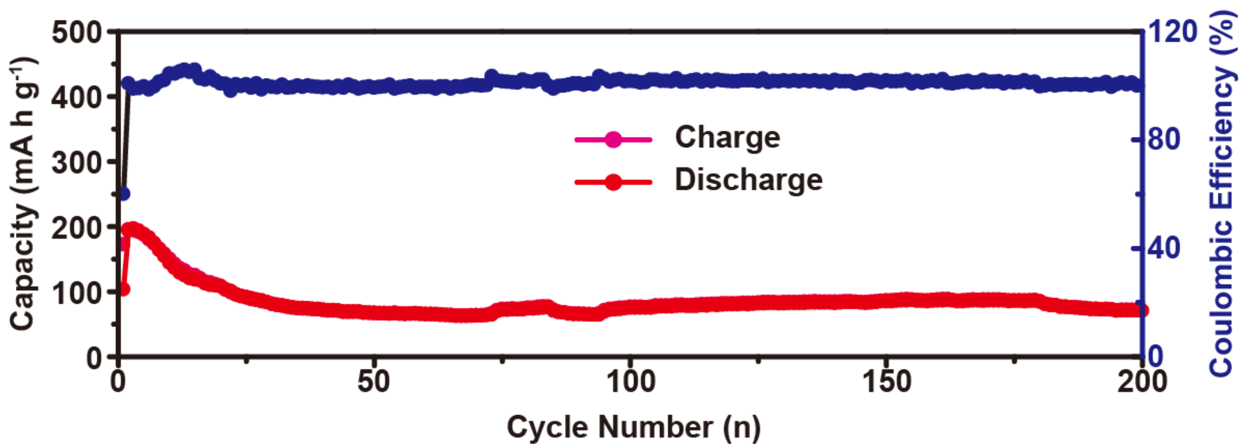

Fig. S8. Cycling performances of δ-MnO_2 electrode using an aqueous electrolyte of 2 M $ZnSO_4$ + 0.2 M $MnSO_4$ at a current density of 500 mA g^{-1}.

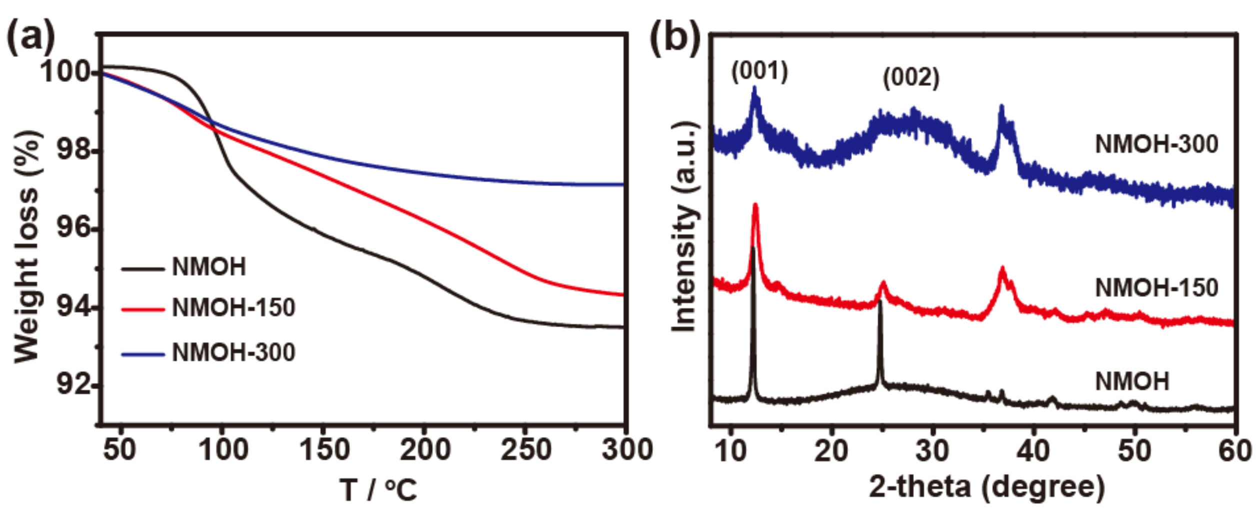

Fig. S9. (a) TGA curves and (b) XRD patterns of NMOH at different thermal treatment temperatures.

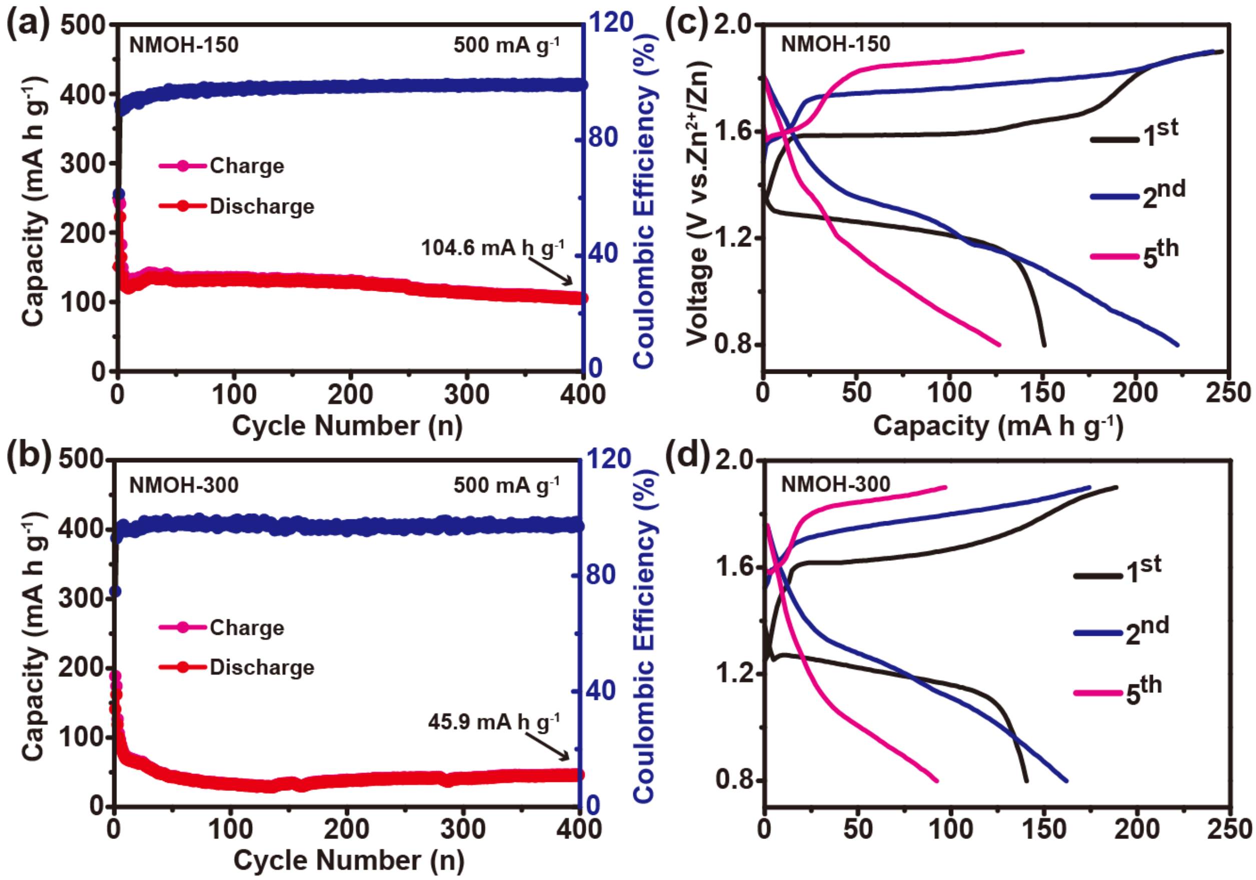

Fig. S10. Cycling performances of (a) NMOH-150, (b) NMOH-300 and corresponding Galvanostatic charge/discharge curves of (c) NMOH-150, (d) NMOH-300 at the current density of 500 mA g^{-1} using an aqueous electrolyte of 2 M $ZnSO_4$ with the 0.2 M $MnSO_4$ additive.

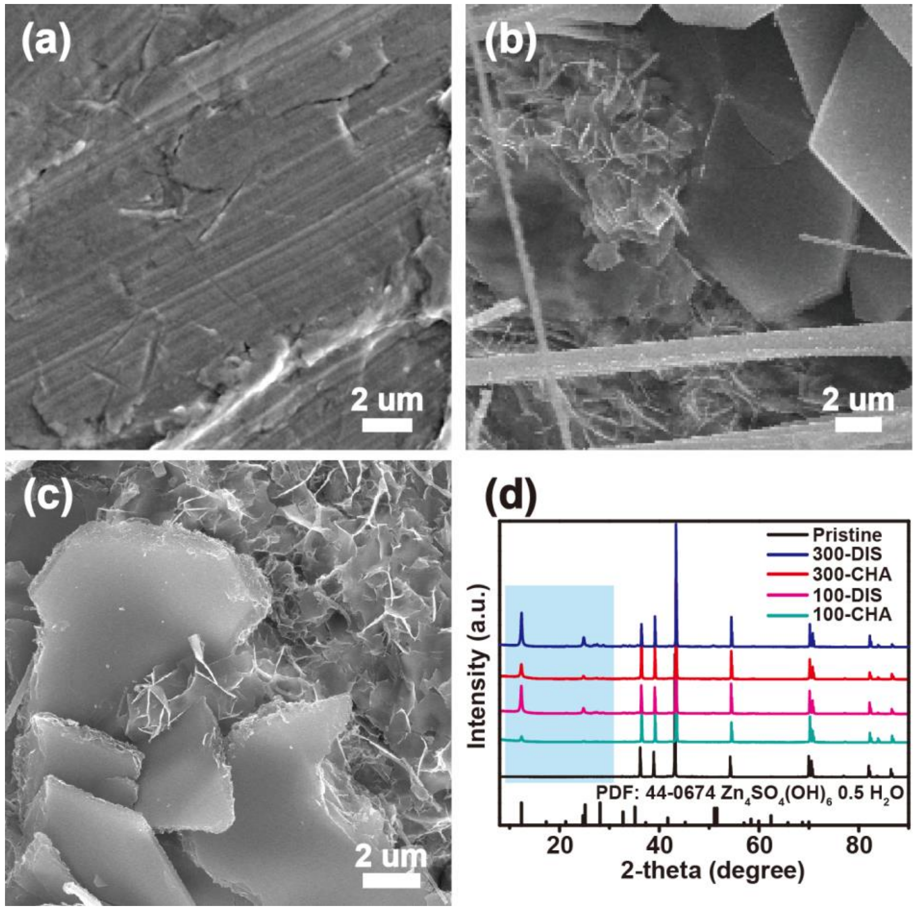

Fig. S11. SEM images of Zn anode at different states: (a) pristine, (b) after 100 cycles, and (c) after 300 cycles. (d) XRD patterns of Zn anode in different cycles. As depicted in Fig. S11 (a-c), the new phase maintained in the Zn anode after 100 cycles. And the microflake should be indexed to the zinc sulfate hydroxide hydrate (Zn_4SO_4 $(OH)_6$ $0.5H_2O$) which will affect the deposition of zinc ions, resulting in the decrease of capacity.

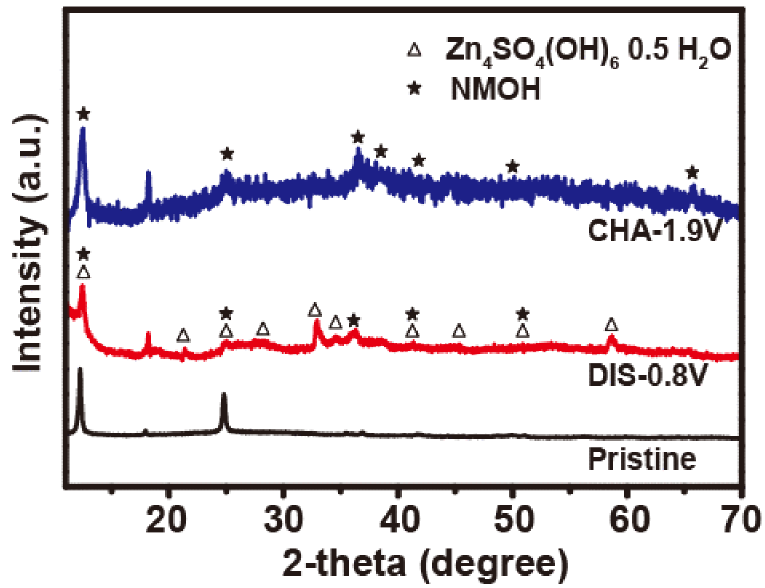

Fig. S12. XRD patterns of the NMOH cathode at different charge/discharge states.

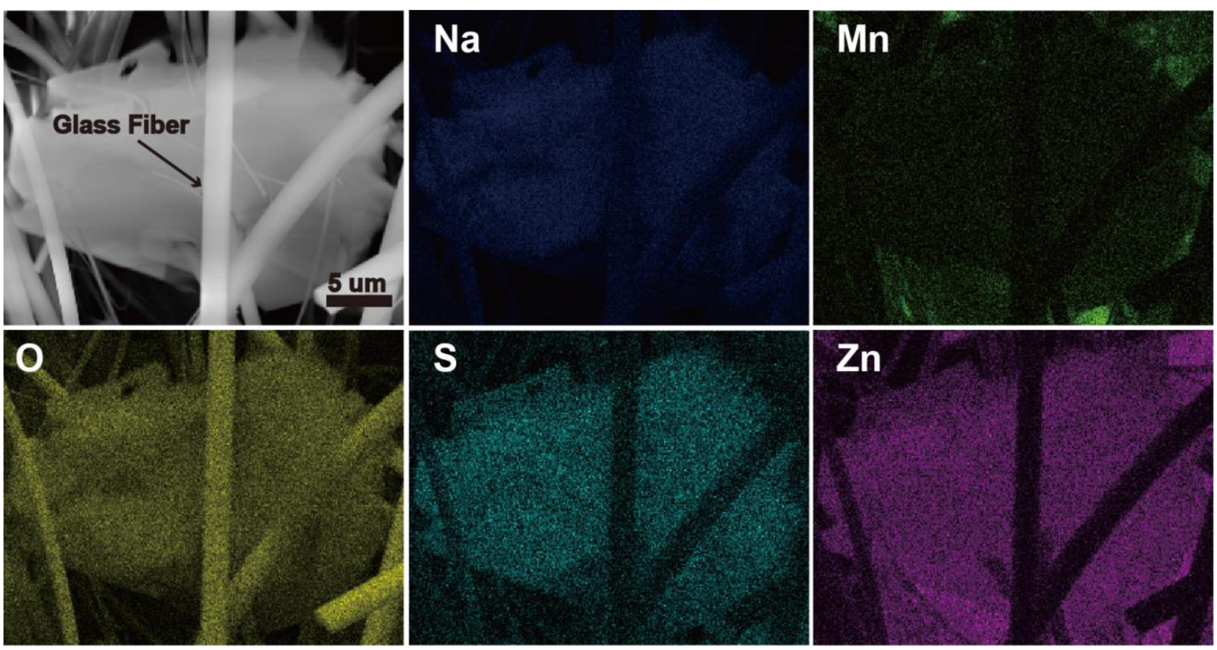

Fig. S13. SEM and elemental mapping images of the new phase at fully discharged state. The fiber-like materials in these images are glass fibers from the separator.

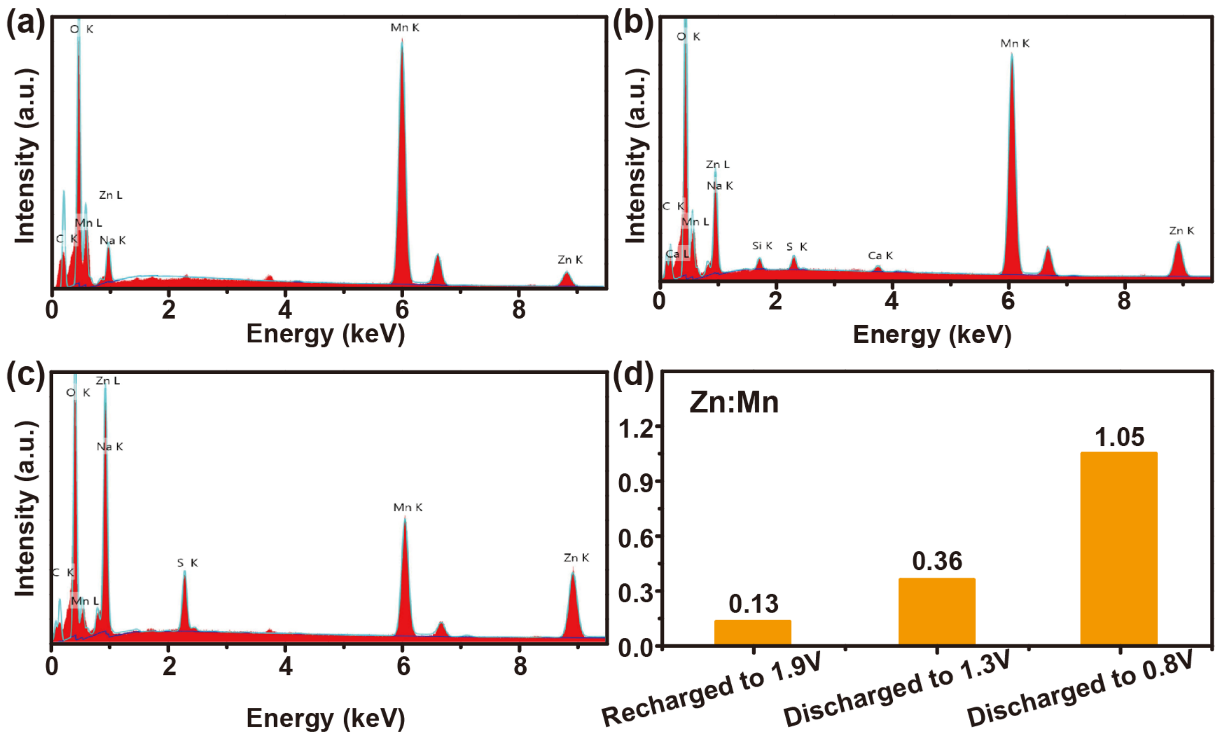

Fig. S14. EDS spectra of the NMOH electrode during the second cycle at 200 mA g^{-1}: (a) charged to 1.9 V, (b) discharged to 1.3 V, and (c) discharged to 0.8 V. (d) Zn/Mn ratios in the electrode at different statuses. Note: the zinc in the ZHS phase is excluded when calculating the ratio of Zn/Mn.

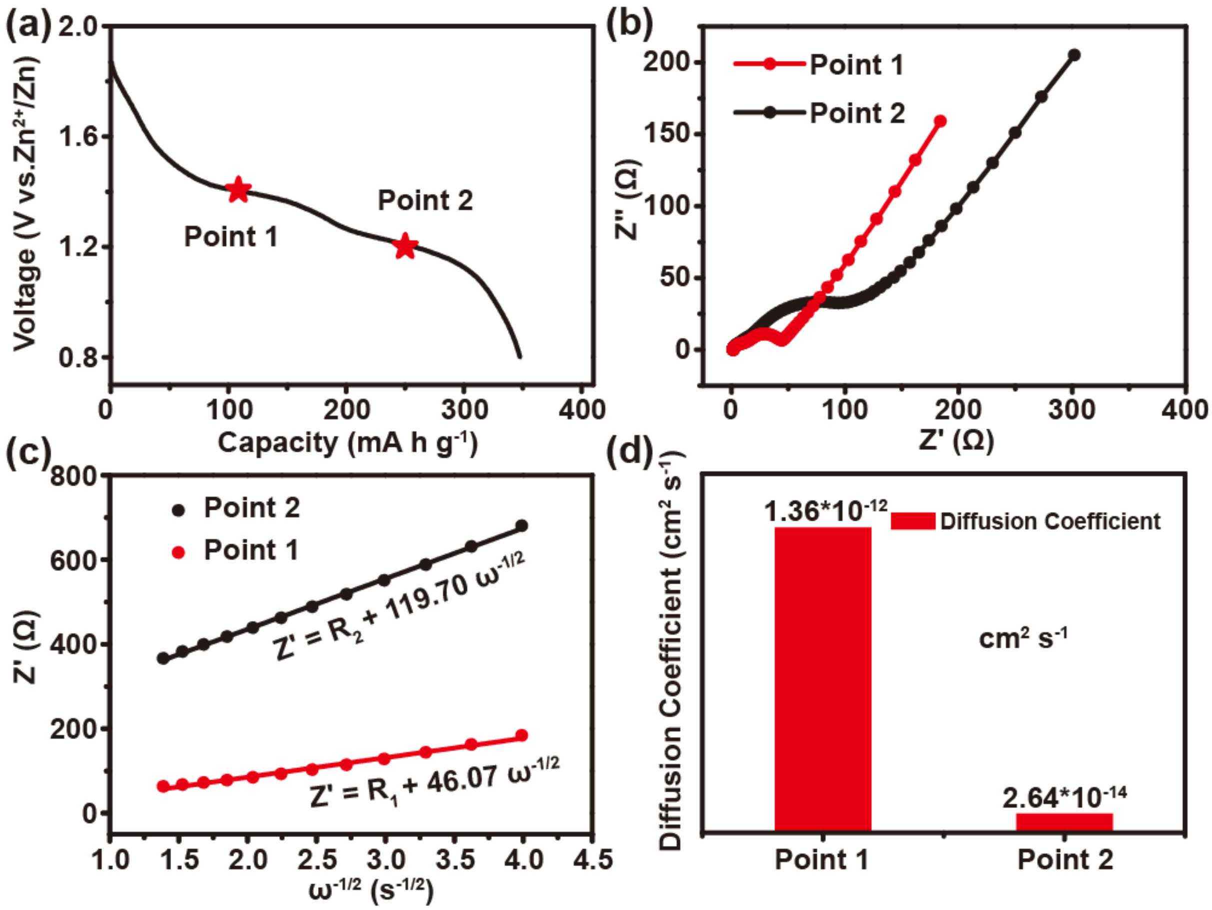

Fig. S15. (a) Typical discharge profile of the Zn/NMOH cell. The points 1 and 2 are collected for EIS test. (b) Nyquist spectra of the cells at the points 1 and 2. (c) Z' vs. $\omega^{-1/2}$ plots of NMOH electrode in the low frequency region. (d) Calculated diffusion coefficients of different discharge platforms. The diffusion coefficient of the Zn/NMOH cell is calculated using the following equation[1]:

$$D = \frac{R^2 T^2}{2A^2 n^4 F^4 C^2 \sigma^2}$$

Where R is the gas constant, T is the experiment temperature, n is the electron number per molecule participating the redox reaction, F is the Faraday constant, A is the surface area of the electrode, C is the molar concentration of insertion ions in NMOH electrode, and σ is the Warburg coefficient calculated from the Z' vs. $\omega^{-1/2}$ plots.

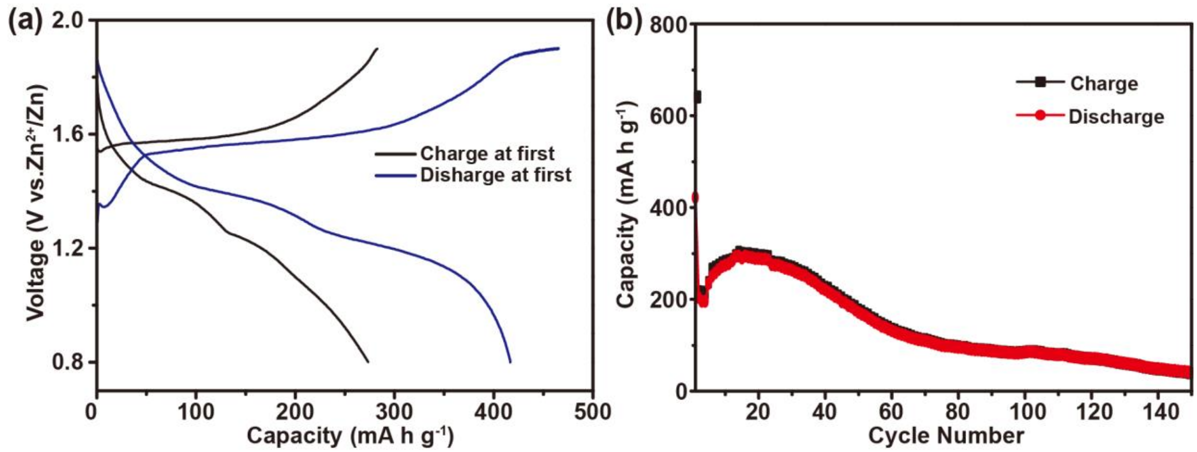

Fig. S16. (a) The 10th galvanostatic charge/discharge curves of the NMOH cathode with different charge and discharge methods at 200 mA g^{-1} between 0.8 and 1.9 V. (b) Cycling performances of the NMOH cathode which charges at first at a current density of 100 mA g^{-1}.

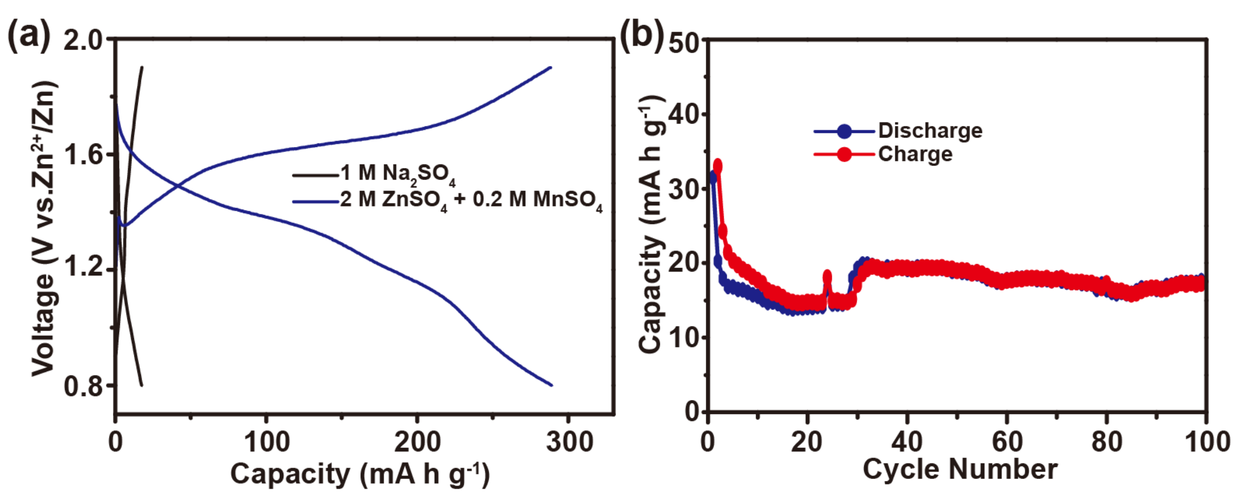

Fig. S17. (a) Typical galvanostatic charge/discharge curves with different electrolytes at 200 mA g^{-1} between 0.8 and 1.9 V of the Zn/NMOH cell. (b) Cycling performances of the Zn/NMOH cell using 1M Na_2SO_4 aqueous electrolyte at a current density of 200 mA g^{-1}.

Table S1. Comparison of electrochemical properties of NMOH with other Mn-based cathode materials reported in the literature.

Cathode Materials	Electrolytes	Specific Capacity/Rate Performance	Refs.
$Na_{0.55}Mn_2O_4 \cdot 0.57\ H_2O$	2 M $ZnSO_4$+0.2 M $MnSO_4$	389.8 mA h g^{-1} at 200 mA g^{-1} 87.1 mA h g^{-1} at 1500 mA g^{-1}	**This work**
$MgMn_2O_4$	1M $MgSO_4$ + 1M $ZnSO_4$ + 0.1M $MnSO_4$	269 mA h g^{-1} at 100 mA g^{-1} 58 mA h g^{-1} at 2400 mA g^{-1}	[2]
MnO_2	1 M $ZnSO_4$	350 mA h g^{-1} at 100 mA g^{-1} -	[3]
$ZnMn_2O_4$/N-doped graphene	1 M $ZnSO_4$+0.05 M $MnSO_4$	221 mA h g^{-1} at 100 mA g^{-1} 75 mA h g^{-1} at 2000 mA g^{-1}	[4]
β-MnO_2	1 M $ZnSO_4$	270 mA h g^{-1} at 100 mA g^{-1} 86 mA h g^{-1} at 1056 mA g^{-1}	[5]
Todorokite-MnO_2	1 M $ZnSO_4$	108 mA h g^{-1} at 50 mA g^{-1} -	[6]
Spinel Mn_3O_4	2 M $ZnSO_4$	239 mA h g^{-1} at 100 mA g^{-1} 51.8% retained at 2000 mA g^{-1}	[7]
MnO_2 on carbon fiber paper	2 M $ZnSO_4$+0.2 M $MnSO_4$	290 mA h g^{-1} at 90 mA g^{-1} 58.6% retained at 1950 mA g^{-1}	[8]
CuHCF	1 M $ZnSO_4$	56 mA h g^{-1} at 20 mA g^{-1} 66.3% retained at 288 mA g^{-1}	[9]
Spinel $ZnMn_2O_4$@C	3 M $Zn(CF_3SO_3)_2$	150 mA h g^{-1} at 50 mA g^{-1} 80 mA h g^{-1} at 500 mA g^{-1}	[10]
ZnHCF@MnO_2	0.5 M $ZnSO_4$	118 mA h g^{-1} at 100 mA g^{-1} 75.2 mA h g^{-1} at 1000 mA g^{-1}	[11]
$ZnMn_2O_4$@PEDOT	1 M $ZnSO_4$	221 mA h g^{-1} at 0.5 mA cm^{-2} 62.5 mA h g^{-1} at 10 mA cm^{-2} (1.66 A g^{-1})	[12]
$ZnMn_2O_4$	1 M $ZnSO_4$+0.5 M $MnSO_4$	106.5 mA h g^{-1} at 100 mA g^{-1} 70.2 mA h g^{-1} at 3200 mA g^{-1}.	[13]
(PANI)-intercalated MnO_2	2 M $ZnSO_4$+0.1 M $MnSO_4$	280 mA h g^{-1} at 200 mA g^{-1} 110 mA h g^{-1} at 3000 mA g^{-1}	[1]

Table S2. ICP-AES results of the sodium ions in 2 M $ZnSO_4$ + 0.2 M $MnSO_4$ electrolytes before and after 2 cycles.

Different status	Na^+ (ppm)
Pristine	6.165
Two cycle	9.148

References

1. J. Huang, Z. Wang, M. Hou, X. Dong, Y. Liu, Y. Wang, Y. Xia, Polyaniline-Intercalated Manganese Dioxide Nanolayers as a High-Performance Cathode Material for An Aqueous Zinc-Ion Battery. Nat. Commun. **9**(1), 2906 (2018). https://doi.org/10.1038/s41467-018-04949-4

2. V. Soundharrajan, B. Sambandam, S. Kim, V. Mathew, J. Jo, S. Kim, J. Lee, S. Islam, K. Kim, Y.-K. Sun, J. Kim, Aqueous Magnesium Zinc Hybrid Battery: An Advanced High-Voltage and High-Energy $MgMn_2O_4$ Cathode. ACS Energy Lett. **3**(8), 1998-2004 (2018). https://doi.org/10.1021/acsenergylett.8b01105

3. K. W. Nam, H. Kim, J. H. Choi, J. W. Choi, Crystal Water for High Performance Layered Manganese Oxide Cathodes in Aqueous Rechargeable Zinc Batteries. Energy Environ. Sci. **12**(6), 1999-2009 (2019). https://doi.org/10.1039/C9EE00718K

4. L. Chen, Z. Yang, H. Qin, X. Zeng, J. Meng, Advanced Electrochemical Performance of $ZnMn_2O_4$/N-doped Graphene Hybrid as Cathode Material for Zinc Ion Battery. J. Power

Sources. **425**, 162-169 (2019). https://doi.org/10.1016/j.jpowsour.2019.04.010

5. S. Islam, M. H. Alfaruqi, V. Mathew, J. Song, S. Kim, S. Kim, J. Jo, J. P. Baboo, D. T. Pham, D. Y. Putro, Y.-K. Sun, J. Kim, Facile Synthesis and the Exploration of the Zinc Storage Mechanism of β-MnO_2 Nanorods with Exposed (101) Planes as a Novel Cathode Material for High Performance Eco-Friendly Zinc-Ion Batteries. J. Mater. Chem. A. **5**(44), 23299-23309 (2017). https://doi.org/10.1039/c7ta07170a

6. J. Lee, J. B. Ju, W. I. Cho, B. W. Cho, S. H. Oh, Todorokite-Type MnO_2 as a Zinc-Ion Intercalating Material. Electrochim. Acta. **112**, 138-143 (2013). https://doi.org/https://doi.org/10.1016/j.electacta.2013.08.136

7. J. Hao, J. Mou, J. Zhang, L. Dong, W. Liu, C. Xu, F. Kang, Electrochemically Induced Spinel-Layered Phase Transition of Mn_3O_4 in High Performance Neutral Aqueous Rechargeable Zinc Battery. Electrochim. Acta. **259**, 170-178 (2018). https://doi.org/https://doi.org/10.1016/j.electacta.2017.10.166

8. W. Sun, F. Wang, S. Hou, C. Yang, X. Fan, Z. Ma, T. Gao, F. Han, R. Hu, M. Zhu, C. Wang, Zn/MnO_2 Battery Chemistry With H^+ and Zn^{2+} Coinsertion. J. Am. Chem. Soc. **139**(29), 9775-9778 (2017). https://doi.org/10.1021/jacs.7b04471

9. Z. Jia, B. Wang, Y. Wang, Copper Hexacyanoferrate with a Well-Defined Open Framework as a Positive Electrode for Aqueous Zinc Ion Batteries. Mater. Chem. Phys. **149-150**, 601-606 (2015). https://doi.org/https://doi.org/10.1016/j.matchemphys.2014.11.014

10. N. Zhang, F. Cheng, Y. Liu, Q. Zhao, K. Lei, C. Chen, X. Liu, J. Chen, Cation-Deficient

Spinel $ZnMn_2O_4$ Cathode in $Zn(CF_3SO_3)_2$ Electrolyte for Rechargeable Aqueous Zn-Ion Battery. J. Am. Chem. Soc. **138**(39), 12894-12901 (2016). https://doi.org/10.1021/jacs.6b05958

11. K. Lu, B. Song, Y. Zhang, H. Ma, J. Zhang, Encapsulation of Zinc Hexacyanoferrate Nanocubes with Manganese Oxide Nanosheets for High-Performance Rechargeable Zinc Ion Batteries. J. Mater. Chem. A **5**(45), 23628-23633 (2017). https://doi.org/10.1039/c7ta07834j

12. H. Zhang, J. Wang, Q. Liu, W. He, Z. Lai, X. Zhang, M. Yu, Y. Tong, X. Lu, Extracting Oxygen Anions from $ZnMn_2O_4$: Robust Cathode for Flexible All-Solid-State Zn-Ion Batteries. Energy Storage Materials. **21**, 154-161 (2019). https://doi.org/https://doi.org/10.1016/j.ensm.2018.12.019

13. X. Wu, Y. Xiang, Q. Peng, X. Wu, Y. Li, F. Tang, R. Song, Z. Liu, Z. He, X. Wu, Green-low-cost rechargeable aqueous zinc-ion batteries using hollow porous spinel ZnMn2O4 as the cathode material. Journal of Materials Chemistry A. **5**(34), 17990-17997 (2017). https://doi.org/10.1039/C7TA00100B